Journal of Power Sources 306 (2016) 559–566

Contents lists available at ScienceDirect

Journal of Power Sources

journal homepage: www.elsevier.com/locate/jpowsour

Binder-free nitrogen-doped carbon paper electrodes derived from polypyrrole/cellulose composite for Li–O_2 batteries

Jia Liu, Zhaohui Wang, Jiefang Zhu*

Department of Chemistry – Ångström Laboratory, Uppsala University, Box 538, SE-751 21 Uppsala, Sweden

HIGHLIGHTS

- The fabrication of NCPE involves cheap raw materials and easy operation.
- The NCPE holds a bird's nest microstructure and N-containing function groups.
- A Li–O_2 cell with NCPE shows a low overpotential and considerable cyclability.
- Using metal-free and binder-free NCPE could avoid some parasitic reactions.
- The metal-free and binder-free electrode design can increase the energy density.

GRAPHICAL ABSTRACT

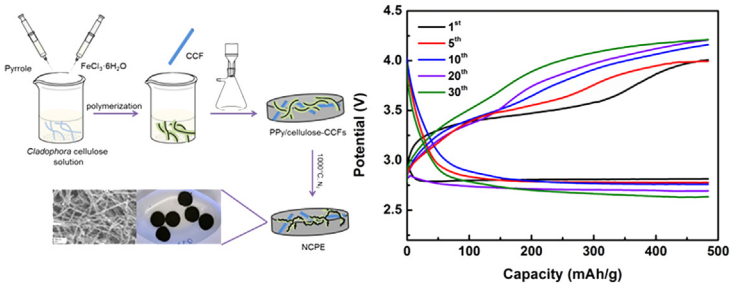

ARTICLE INFO

Article history:
Received 15 December 2015
Accepted 16 December 2015
Available online xxx

Keywords:
Nitrogen-doped carbon paper electrode
Binder-free
Free-standing
Li–O_2 battery
Bird's nest microstructure
N-containing functional group

ABSTRACT

This work presents a novel binder-free nitrogen-doped carbon paper electrode (NCPE), which was derived from a N-rich polypyrrole (PPy)/cellulose-chopped carbon filaments (CCFs) composite, for Li–O_2 batteries. The fabrication of NCPE involved cheap raw materials (*e.g., Cladophora* sp. green algae) and easy operation (*e.g.,* doping N by a carbonization of N-rich polymer), which is especially suitable for large-scale production. The NCPE exhibited a bird's nest microstructure, which could provide the self-standing electrode with considerable mechanic durability, fast Li^+ and O_2 diffusion, and enough space for the discharge product deposition. In addition, the NCPE contained N-containing function groups, which may promote the electrochemical reactions. Furthermore, binder-free architecture designs can prevent binder-involved parasitic reactions. A Li–O_2 cell with the NCPE displayed a cyclability of more than 30 cycles at a constant current density of 0.1 mA/cm^2. The 1st discharge capacity for a cell with the NCPE reached 8040 mAh/g at a current density of 0.1 mA/cm^2, with a cell voltage around 2.81 V. A cell with the NCPE displayed a coulombic efficiency of 81% on the 1st cycle at a current density of 0.2 mA/cm^2. These results represent a promising progress in the development of a low-cost and versatile paper-based O_2 electrode for Li–O_2 batteries.

1. Introduction

The rechargeable Li–O_2 battery has recently attracted a great deal of attention because of its significantly higher theoretical energy density than traditional lithium-ion battery [1,2,4,5]. A Li–O_2

* Corresponding author.
E-mail address: jiefang.zhu@kemi.uu.se (J. Zhu).

http://dx.doi.org/10.1016/j.jpowsour.2015.12.074
0378-7753/

battery prototype is composed of a lithium metal anode, Li^+-containing nonaqueous electrolyte, and a porous O_2 cathode (normally carbon-based materials with or without catalysts). The key electrochemical reaction in a Li–O_2 battery is $2Li + O_2 \rightleftarrows Li_2O_2$, with a discharge process (oxygen reduction reaction (ORR)) and a charge process (oxygen evolution reaction (OER)) [6]. Although Li–O_2 batteries exhibit a great potential and much progress has been made, the main issues to be addressed are: 1) How to find a long-term stable electrolyte with high O_2 solubility and diffusion; 2) How to design a stable O_2 electrode with excellent electrocatalysts; 3) How to prevent the dendrite formation on the Li metal surface; 4) How to protect the electrodes from CO_2 and H_2O.

The energy storage capacity, rate capacity, and cycle life are strongly determined by the materials and architecture of the O_2 electrode [8]. Carbonaceous materials have been employed as fillers to provide the cathode with porosity and electronic conductivity [9]. It has been well established that a good carbon candidate for Li–O_2 batteries should have characteristics as follows: i) appropriate pore size/volume; ii) large surface area, and iii) high stability. So far, various carbon materials have been systematically studied for Li–O_2 batteries, such as commercial carbon powders [10], one-dimensional carbon nanomaterials [11], two-dimensional graphene [12], mesoporous carbon materials [13], and carbon hybrids and composites [14–16]. To promote the electrochemical performance, the incorporation of heteroatoms in a well-defined way is regarded as a feasible strategy to modify the nature and chemical properties of pure carbon [9]. Among those heteroelements, nitrogen (N), having a comparable atomic size to carbon and five valence electrons for bonding with the carbon atom, has been widely adopted [17,18]. N-doped carbon can not only improve the Li + diffusion and transfer by generating defects and by withdrawing electrons from the carbon atom, but also increase the conductivity of the resulting carbon, which can exhibit a better battery performance than pure carbon materials [19–22]. Many approaches have been reported for the synthesis of N-doped carbon [22–24]. Those synthetic routes normally require multiple or complicate steps, with low yield and high cost, which inevitably limit large-scale fabrication. Therefore, to obtain high-performance N-doped carbon by an easy-to-operate and low-cost method is really a challenge.

Besides the stability of electrolyte, the composition and architecture of the O_2 electrode also influences the performance of Li–O_2 batteries. Typically, a N-doped carbon-based electrode consists of N-doped carbon powder, polymer binder, and catalyst. The multiple components complicate the cell preparation and the electrochemical reactions, and also impose the challenges on the analysis. In addition, carbon particles in an electrode using chemical binder sometimes display a tight aggregation, which inevitably decreases the O_2 diffusion and limits the space for Li_2O_2 deposition. This consequently leads to a limited capacity and a low energy efficiency of the Li–O_2 battery [25]. Moreover, the binder degradation can clog the O_2 electrode surface and then reduce the space for the desired discharge product Li_2O_2 [7]. Binder-free O_2 electrode, designed to avoid the negative influence of the binder, has been reported and recognized as an appealing alternative for Li–O_2 batteries [18,25,27–29]. We have developed a straightforward approach to the manufacture of sustainable paper electrodes based on a high-porous polypyrrole (PPy)/*Cladophora* cellulose composite, and thus the possibility to use the carbonized derivative as binder-free electrodes for Li–O_2 batteries is highly appealing [30–33].

Herein, we report a novel design of a binder-free N-doped carbon paper electrode (NCPE) in the Li–O_2 battery derived from a N-rich PPy/cellulose-chopped carbon filaments (CCFs) composite. The synthetic strategy combines the low-cost and easily accessible raw materials, and a facile operation. The NCPE displays a bird's nest microstructure, which can provide the electrode with considerable mechanic durability, fast Li^+ and O_2 diffusion, and enough space for the discharge product deposition. The rate performance, coulombic efficiency, and cyclability of the Li–O_2 batteries with NCPEs were investigated. The function of the NCPEs is related to their N-containing function groups and self-standing bird's nest microstructure. We expect that this new designed NCPE can be manufactured and used as an electrode material for broad applications (*e.g.,* Li-ion batteries, fuel cells, supercapacitors, *etc.*).

2. Experimental

2.1. Materials

All chemicals were of analytic grade and used as received without any further purification. *Cladophora* green algae was collected from the Baltic Sea, and the *Cladophora* nano-cellulose was extracted from the algae by grinding and acid hydrolysis as previously described [34]. Iron (III) chloride nonahydrate ($FeCl_3 \cdot 6H_2O$), hydrochloric acid (HCl) and pyrrole (Py) were purchased and used as delivered from Sigma-Aldrich. The carbon filaments (CFs) were obtained from Goodfellow, UK. The CFs were simply chopped with a kitchen herb-cutter knife on a wooden block so as to obtain a fluffy mass consisting of individual CCFs with a maximum length of 5 mm. 1 M lithium perchlorate ($LiClO_4$, GFS, $\geq$ 99%) in dimethyl sulfoxide (DMSO, Aldrich, $\geq$ 99.9%) was prepared as electrolyte in the Li–O_2 battery.

2.2. Preparation of the NCPE

Cladophora cellulose (200 mg) was dispersed in water (40 mL) by sonication for 10 min with water cooling. The sonication was carried out with a high-energy ultrasonic equipment (Sonics and Materials Inc., USA, Vibra-Cell 750) at an amplitude of 30% with a pulse length of 30 s and pulse-off duration of 30 s. Pyrrole (0.65 mL) and 0.5 M HCl (40 mL) were mixed with the cellulose dispersion by magnetic stirring for 5 min. PPy was then formed on the *Cladophora* cellulose fibers *via* polymerization with $FeCl_3 \cdot 6H_2O$ (5.9 g) dissolved in 0.5 M HCl (40 mL) as an oxidant. The polymerization proceeded for 30 min under stirring, after which the composite was collected in an Büchner funnel connected to a suction flask, and washed with 0.5 M HCl (3 L) and 0.1 M HCl (0.5 L). The PPy/cellulose composite precursor has been extensively characterized in our previous work [30–32]. The PPy/cellulose composite and 200 mg of CCFs were suspended in 200 mL of water using a mechanical homogenizer (IKA T25 Ultra-Turrax, Germany) at 6200 rpm for 10 min. The mixture was drained on a polypropylene filter and then dried to form a PPy/cellulose-CCFs paper sheet. As-prepared paper was heated to 1000 °C at a heating rate of 3 °C/min and kept for 1 h under a nitrogen atmosphere to form the NCPE. The schematic illustrating of the synthetic procedure of the NCPE is shown in Scheme 1. The obtained NCPE was then punched into a disc with a diameter of 1.2 cm for directly using as an O_2 electrode (Fig. S1a in Supplementary Information (SI)). In addition, in order to investigate the influence of the doping N on the Li–O_2 battery performance, a reference precursor of cellulose-CCFs paper sheet was also prepared under the similar conditions without the addition of PPy. Thus an undoped carbon paper electrode was obtained after annealing.

2.3. Preparation of a reference electrode based on the chopped NCPE powder and binder

In order to study the effect of binder-free architecture on the

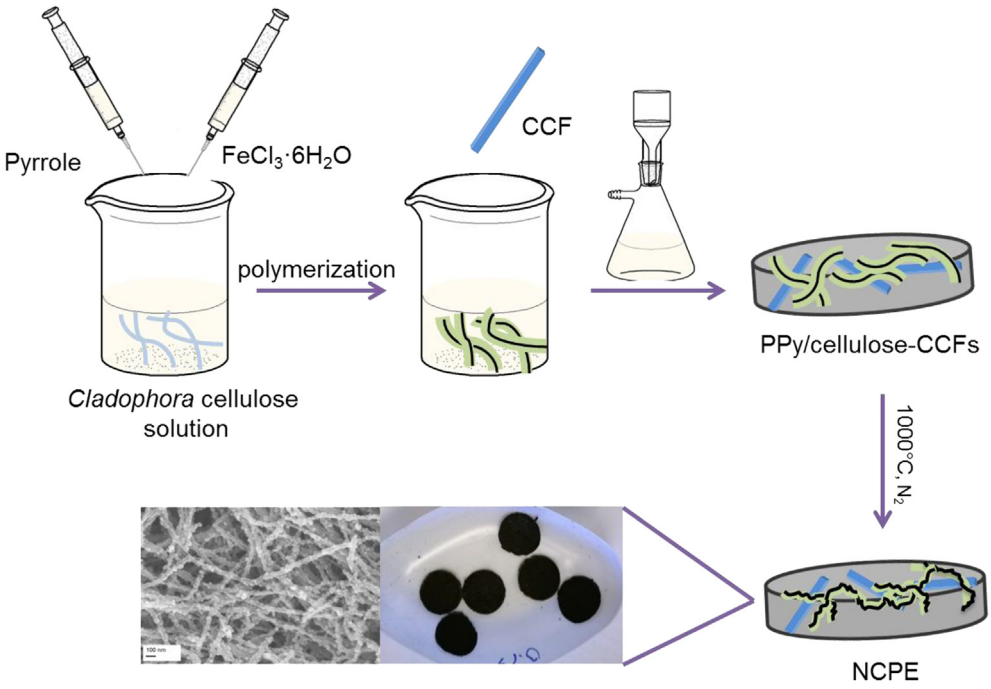

Scheme 1. Schematic illustrating of the synthetic procedure of the NCPE.

$Li-O_2$ battery performance, the NCPE was chopped into powder and mixed with binder to prepare a reference electrode. The chopped NCPE powder and Kynar 2801 (a copolymer based on PVdF, Arkema) were mixed with acetone solvent (≥99.0%, Fluka) in a weight ratio of 90:10 by the high energy ball-milling for 1 h to prepare a slurry. This slurry was then cast drop-wise onto an aluminum mesh substrate with a diameter of 1.2 cm. After acetone evaporation, an electrode based on the chopped NCPE powder and binder was obtained.

2.4. Assembly of $Li-O_2$ battery and electrochemical testing

As-prepared NCPE and the electrode made of chopped NCPE powder and binder were transferred to a vacuum furnace (Buchi Glass Oven B-585) in an Ar-filled glove box (H_2O and O_2 < 1 ppm), and dried at 120 °C overnight. The $Li-O_2$ batteries were assembled in a Swagelok design modified to allow pure and dry O_2 to access through the electrode, which were set up in O_2-filled bottles (Figs. S1b–d in SI). The O_2 pressure inside the bottle during the battery operation was 1 atm, and the volume of O_2 was 300 mL, which was 100 times more than the required amount for the discharge process. The components followed as: Li foil anode, double-layer Solupor separator presoaked in the electrolyte (1 M $LiClO_4$/DMSO), and the NCPE or the chopped NCPE powder and binder-based cathode. The weight of each cathode was 4.5–6.5 mg. The electrochemical measurements were carried out using a Digatron BTS-600 battery system at galvanostatic current densities (0.1 mA/cm^2 (corresponding to ~ 35 mA/g based on the N-doped carbon weight for the NCPE), 0.2, 0.4, and 0.8 mA/cm^2) within a potential range of 2.2–4.5 V *vs.* Li^+/Li.

2.5. Characterization

The XRD analysis of NCPE was made by a Bruker D8 TwinTwin X-ray diffractometer (XRD), operating at 40 mA and 40 kV, using Cu Kα radiation (wavelength (λ) = 1.5406 Å). The Raman spectrum was recorded on a RENISHAW inVia Raman Microscrope at room temperature, with an excitation laser wavelength (λ) of 633 nm. The BET surface area and porosity were determined by a nitrogen adsorption apparatus (Micromeritics ASAP 2020). Thermogravimetry (TG) measurement was performed on a TGA Q500 thermogravimetric analyzer from room temperature to 1000 °C at a heating rate of 10 °C/min under the N_2 flow to study the pyrolysis process of the prepared PPy/cellulose and PPy/cellulose-CCFs. The morphology, particle size and element analysis were carried out by a scanning electron microscopy coupled with an energy dispersive spectroscopy (SEM/EDS-Zeiss 1550 with Aztec EDS). X-ray photoelectron spectroscopy (XPS) measurement was performed by a Perkin Elmer PHI 5500 spectrometer, using monochromatized Al Kα radiation (hν = 1486.7 eV) and an emission angle of 45°.

3. Results and discussion

The XRD pattern of the NCPE is shown in Fig. 1a. The diffraction peaks at 2θ = 25.5° and 42.7° are indexed to the (002) and (101) reflections of graphitic carbon (JCPDS No. 00-023-0064), respectively [35]. Note that the XRD pattern of the N-doped carbon obtained *via* a pyrolysis process of PPy/cellulose precursor showed the similar result (Fig. S2 in SI), indicating that the diffraction peaks in Fig. 1a mainly correspond to the N-doped carbon in NCPE instead of the CCFs. Fig. 1b shows the Raman spectrum of the NCPE. The band at 1373 cm^{-1} (D-band) originates from defect-induced mode [19], while the band at 1575 cm^{-1} (G-band) corresponds to well-graphitized carbon [21], which agrees well with the XRD result. Fig. 1c shows the N_2 adsorption/desorption isotherm curves for the NCPE, which display the mesoporous structure (type IV shape) and which yield a surface area of 107 m^2 g^{-1}. The NCPE has a pore size distribution in the range of 1–65 nm (Inset of Fig. 1c). TG analysis not only characterizes the pyrolytic treatment, but also provides a feasible means for the quantitative analysis of the NCPE components. The NCPE was prepared by a simple carbonization of a PPy/cellulose-CCFs composite, during which process CCFs kept the

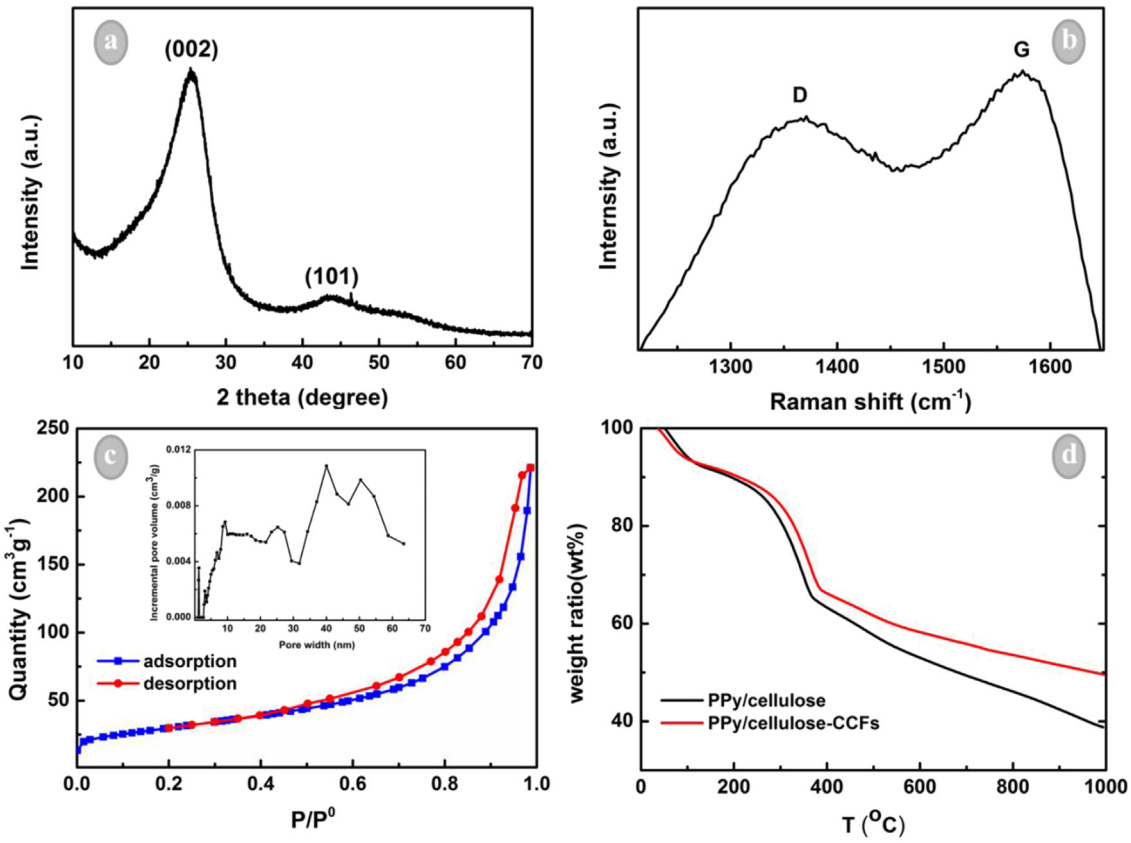

Fig. 1. (a) XRD pattern, (b) Raman spectrum, (c) N_2 adsorption/desorption isotherm curves (Inset: the pore size distribution) of the NCPE, and (d) TG curves of PPy/cellulose and PPy/cellulose-CCFs samples.

same weight. In order to quantify the content of N-doped carbon obtained after the pyrolysis of the PPy/cellulose precursor, the PPy/cellulose (without CCFs) was also prepared under the similar conditions. Fig. 1d shows the TG curves of PPy/cellulose and PPy/cellulose-CCFs samples. Note that the weight changes of the PPy/cellulose and PPy/cellulose-CCFs samples have similar trends and the pyrolytic process of a N-rich polymer composite can be divided into three steps, which is in good agreement with the literature [36]. Step I (35–120 °C) corresponds to the loss of residual water in the samples. Step II (120–380 °C) is assigned to the loss of volatile components, accompanied by the C–O bond cracking [37]. Step III (380–1000 °C) is the carbonization period, connecting with the C–H bond breaking [38]. There are 64 wt% of N-doped carbon and 36 wt% of CCFs in the NCPE, based on the TG results (the estimation follows the equations S1–S4 in SI).

The functional composition of final chemical product, NCPE is N-doped carbon with CCFs. The employment of CCFs can not only provide considerable conductivity and mechanical strength for the NCPE, but also support the self-standing electrode as a skeleton. Note that the sample without CCFs was very fragile. Fig. 2 presents SEM images of the NCPE and the corresponding EDS elemental mapping of C, N, and O. As depicted in Fig. 2a, the CCFs, which show an average length of 1 mm, are embedded in the NCPE. The morphology and size of CCF were not changed during the annealing (see Fig. S3 in SI). During synthesis, the cellulose in the PPy/cellulose-CCFs composite acted as a structural and substrate template for the PPy coating [33]. Then, the N-doped carbon in the NCPE was obtained *via* a pyrolytic treatment of PPy/cellulose composite precursor. The N-doped carbon in the NCPE exhibited a bird's nest microstructure consisting of branches with a width of ~70 nm (Fig. 2b–d). The branch surface was very rough, due to the pyrolysis treatment of the PPy [39]. This bird's nest architecture with stable integrity can provide the self-standing cathode with mechanic durability, fast O_2 diffusion, and enough space for discharge product deposition, as well-studied by previous reports [18,40]. As presented in Fig. 2e, CCFs show the smooth surface with a diameter of ~7 μm. The N-doped carbon seems firmly attached to the CCFs. From the EDS elemental mapping, the CCFs mainly consist of the C element (Fig. 2f), while the N-doped carbon is composed of well-dispersed C, N and O elements (Fig. 2f and g), indicating that doping N *via* the pyrolysis of a N-rich polymer composite was successful.

The chemical states and surface compositions of the NCPE were studied by XPS. Fig. 3a displays the survey spectrum (0–600 eV) of the NCPE, which basically includes C, N, and O without any other impurities. The amount of doped N for the NCPE was ~7 wt%, based on the XPS results. The N1s spectrum for the NCPE contained two peaks at 397.7 and 400.4 eV, as shown in Fig. 3c, which were in good agreement with the binding energies of the pyridinic and pyrrolic N [22,41], respectively. Therefore, it is evident that nitrogen atoms were doped into the carbon lattice instead of dangling on the carbon surface. The PPy consists of five-membered pyrrole rings, which can be partly converted to six-membered pyridine rings during pyrolysis. These N-containing groups introduce the high positive spin density and asymmetry atomic charge density, resulting in the formation of defects and/or vacancies, which can promote the electrochemical reactions [17,42–45].

The capacities were calculated based on the weight of the N-doped carbon in the NCPE, since the capacity of a reference cell excluding PPy could be neglected (see Fig. S4 in SI), meaning that

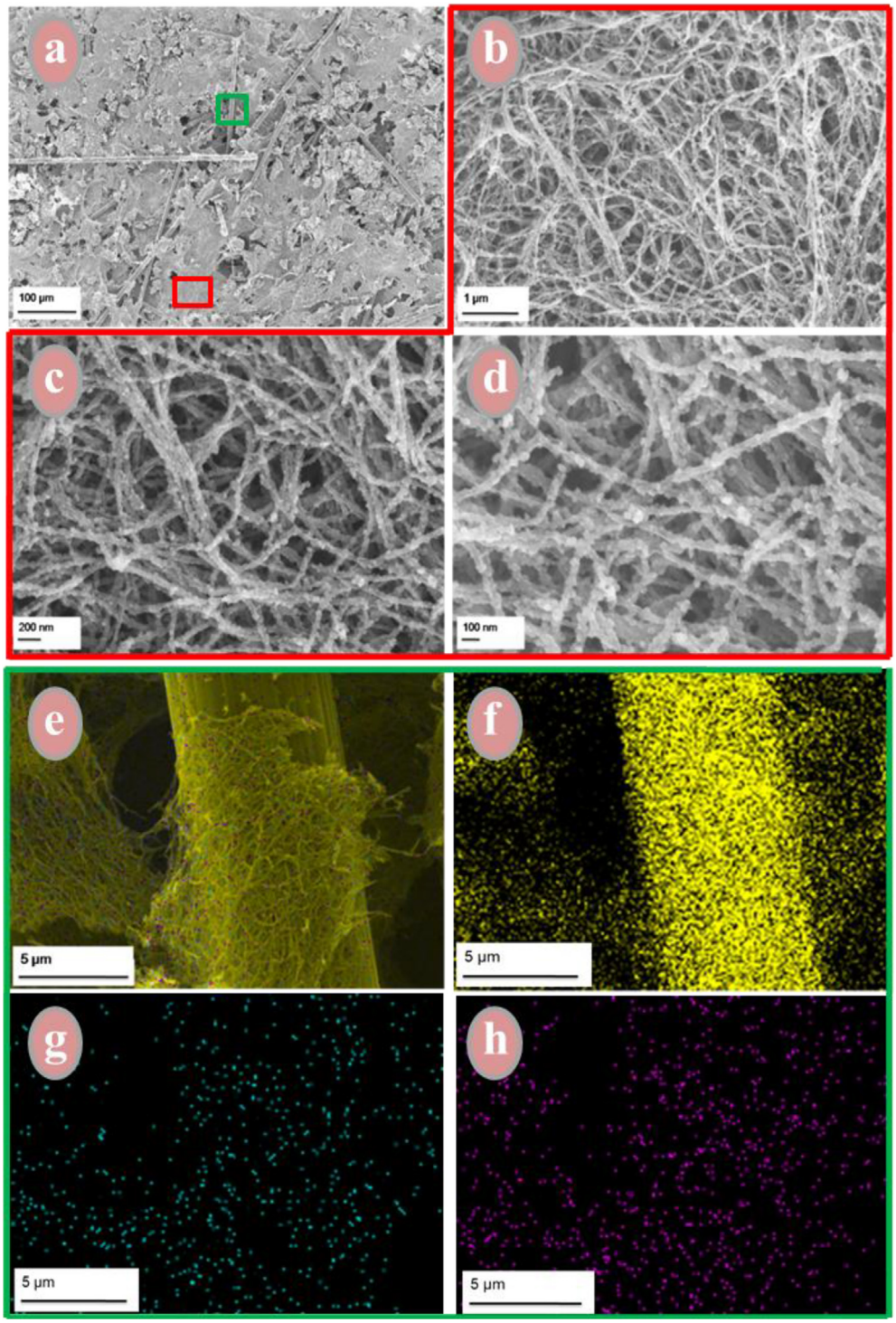

Fig. 2. (a) SEM image of the NCPE, (b–d) SEM images of the region enclosed by the red frame in (a), (e) SEM image of the region enclosed by the green frame in (a), EDS elemental mapping of (f) C, (g) N, and (h) O in the SEM image (e). (For interpretation of the references to colour in this figure legend, the reader is referred to the web version of this article.)

CCFs do not contribute to any capacity. The discharge profiles of Li–O_2 batteries with NCPEs at different current densities ranging from 0.1 to 0.8 mA/cm^2 are shown in Fig. 4a. It can be seen that the 1st discharge capacity of a cell at a current density of 0.1 mA/cm^2 reached 8040 mAh·g^{-1}. The achieved capacity and operating potential decreased with increasing current density. When higher current densities of 0.2, 0.4 and 0.8 mA/cm^2 were used, the 1st discharge capacities were 4759, 2147, and 419 mAh·g^{-1}, respectively. The specific area resistance of the NCPE was around 267 Ω cm^2 (the estimation follows the equation S(5) in SI). The galvanostatic discharge/charge curves on the 1st cycle for a Li–O_2 battery at a current density of 0.2 mA/cm^2 is shown in Fig. 4b. The discharge and charge capacities were 4759 and 3865 mAh·g^{-1} respectively, indicating that this cell exhibited a coulombic efficiency of 81%. The cyclability and rate performance of Li–O_2 batteries with NCPEs under a capacity limit of 480 mAh·g^{-1} at various

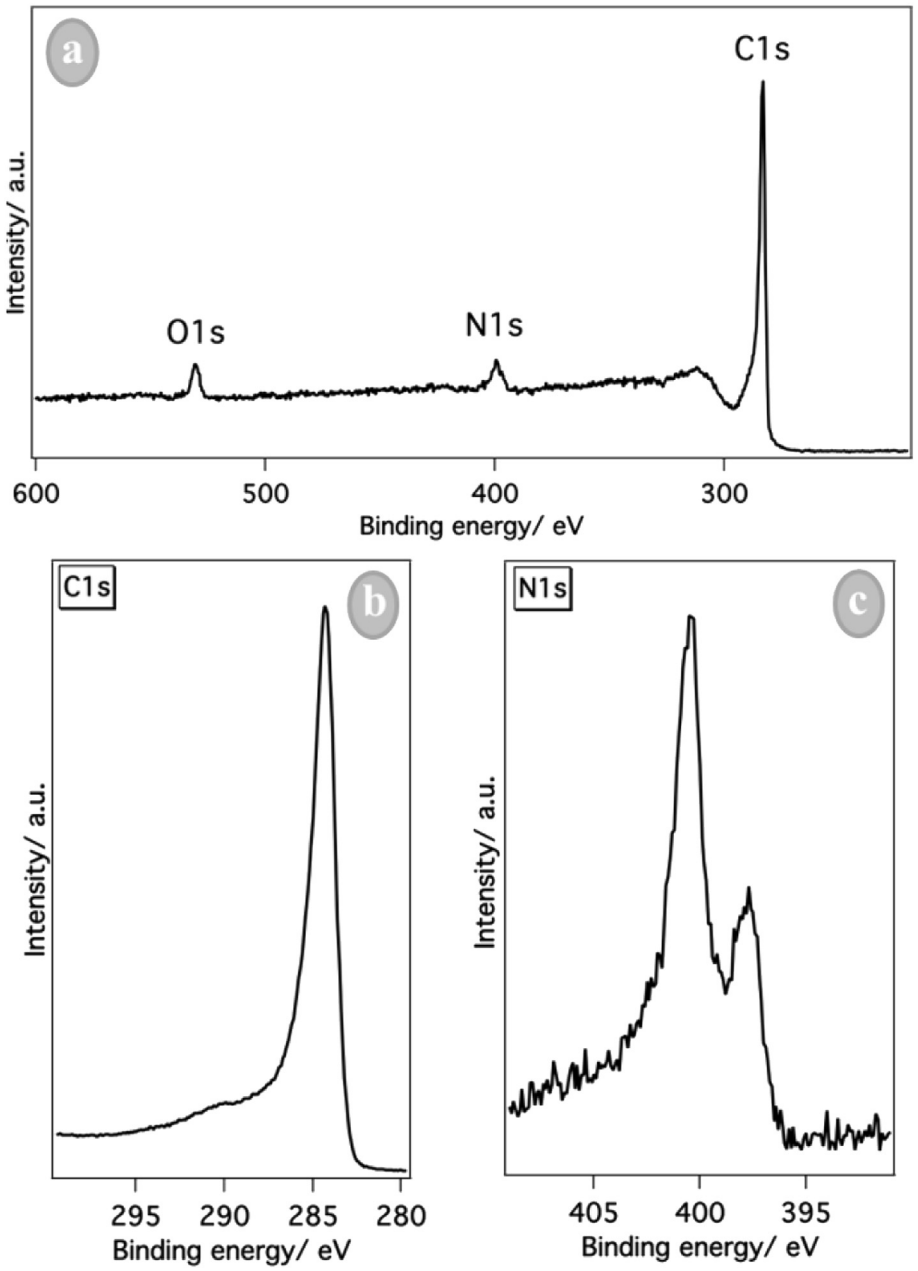

Fig. 3. (a) XPS survey spectrum, (b) C1s and (c) N1s core level spectra of the NCPE.

current densities (0.1–0.4 mA/cm^2) were evaluated *via* time-controlled and voltage-controlled modes. As shown in Fig. 4c, a Li–O_2 cell with the NCPE presented a cyclability of more than 30 cycles at a current density of 0.1 mA/cm^2. Note that there were two potential stages during the charge process. The first could be assigned to the Li_2O_2 oxidation, while the other may correspond to electrolyte decomposition [46,47], and/or the LiOH oxidation [5]. LiOH could be formed due to the introduction of water into the system *via* the DMSO solvent, and/or the DMSO oxidation by reactive oxygen species (*e.g.*, LiO_2 and Li_2O_2) [48,49]. Note that it shows a much lower overpotential of 0.68 V for the 1st cycle than that of around 1.2–1.5 V with only super P/binder-based electrode [50], indicating that the employment of NCE can effectively reduce the overpotential of the Li–O_2 cell. This could give an explanation that the metal and binder-free self-standing NCE prevents or reduces the side reactions (i.e. decomposition of binder or electrolyte). The overpotentials increased gradually with the cycle number, mainly due to the increased charge potentials. In addition, the discharge capacity dropped after 30 cycles (Fig. S5a in SI). Besides the fact that DMSO is not completely stable, the instability of contact interface between Li metal and DMSO could be another reason for the sudden death of the battery [51,52] (see Fig. S6 in SI). The batteries sustained 14 and 5 cycles with a capacity limit of 480 mAh·g^{-1} at constant current densities of 0.2 and 0.4 mA/cm^2, respectively (Figs. S5b and 5c in SI). The cell overpotential on the 1st cycle increased from 0.68 to 0.99 V, when raising the current density from 0.1 to 0.4 mA/cm^2 (Fig. 4c–e).

In order to know how the unique architecture of the NCPE benefits the battery performance, the cycling response of a Li–O_2 battery with a reference electrode based on chopped NCPE powder and binder was studied, as shown in Fig. 4f. It can be seen that the cell overpotential (1.34 V) on the 1st cycle was much higher than

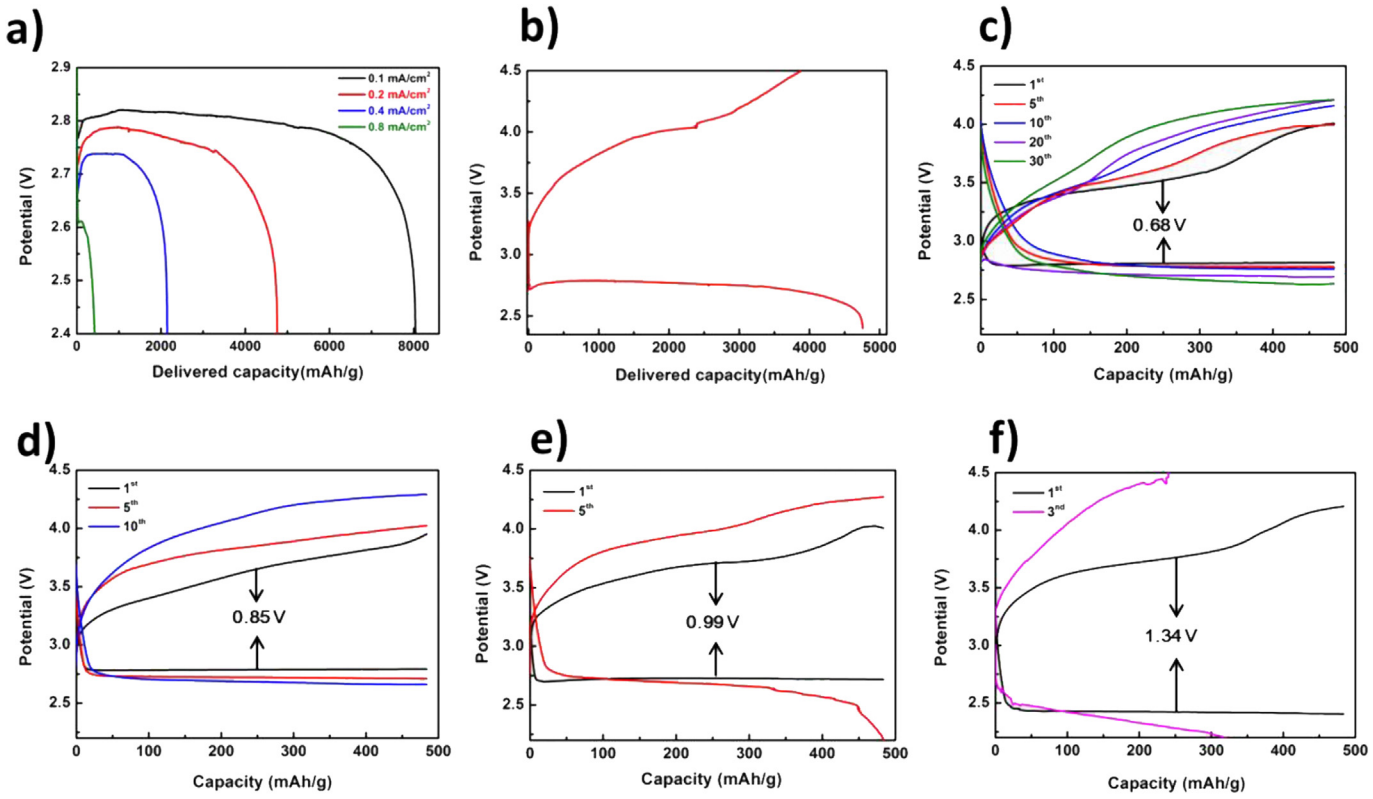

Fig. 4. (a) The discharge profiles for Li–O_2 batteries with NCPEs at various current densities of 0.1, 0.2, 0.4 and 0.8 mA/cm^2 with a cut off voltage of 2.4 V, (b) discharge/charge profiles on the 1st cycle for a Li–O_2 battery with the NCPE at a current density of 0.2 mA/cm^2 within a potential range of 2.4–4.5 V *vs.* Li^+/Li, and the cycling response of the Li–O_2 batteries with NCPEs at constant current densities of (c) 0.1, (d) 0.2, (e) 0.4 mA/cm^2, and (f) cycling response of a Li–O_2 battery with a reference electrode based on the chopped NCPE powder and binder at a constant current density of 0.2 mA/cm^2 under a specific capacity limit of 480 mAh/g (based on the weight of N-doped carbon) within a potential range of 2.2–4.5 V *vs.* Li^+/Li.

that (0.85 V) for a cell with the NCPE. Additionally, the battery only sustained 2 cycles with a capacity limit of 480 mAh·g^{-1}, and there was an obvious capacity loss on the following 3rd cycle. There can be two possible reasons for this poor cyclability. One is that an aggregation of electrode materials due to the binder addition impeded the O_2 diffusion and limited the Li_2O_2 deposition space, which was supported by the SEM image of this binder-containing electrode (Fig. S7 in SI). The other may be that the binder-involved side reactions interfered with the electrochemical processes. This experiment confirms the advantages of bird nest's structure and binder-free design.

Since pyrrole is the N precursor in this work, the only way to study the N-doping effect is to exclude pyrrole (*i.e.*, without the formation of PPy before carbonization) in the synthesis. The cell with the electrode excluding PPy showed very low capacity (Fig. S4 in SI), indicating that N groups and other components formed *via* the carbonization of PPy are important functional materials for Li–O_2 battery.

4. Conclusion

The fabrication of NCPE can be considered as a green chemistry process, since it uses cheap raw materials (*e.g.*, *Cladophora* sp. green algae) and involves easy operations (*e.g.*, doping N *via* the pyrolysis of a N-rich polymer composite). The NCPE displays a bird's nest microstructure, which could provide the self-standing electrode with mechanic durability, fast O_2 diffusion, and enough space for discharge product deposition. The N-doped carbon in the NCPE provided the N-containing function groups, which can promote the electrochemical reactions. The 1st discharge capacity for a Li–O_2 cell with the NCPE at the current density of 0.1 mA/cm^2 reached 8040 mAh·g^{-1} with a cell voltage around 2.81 V. In addition, the cell with the NCPE presented a cyclability of more than 30 cycles at a constant current density of 0.1 mA/cm^2. It exhibited a coulombic efficiency of 81% on the 1st cycle at the current density of 0.2 mA/cm^2. We think that this new designed NCPE can make a contribution to improving the energy density (without metal and binder) and preventing some parasitic reactions (*e.g.*, from binder degradation) for Li–O_2 batteries.

Acknowledgments

This work is supported by Swedish Research Council (2012-4681), Swedish Energy Agency, Ångpanneföreningen's Foundation for Research and Development, J. Gust. Richert Foundation, and the State Key Laboratory of Fine Chemicals (KF1413). Reza Younesi is gratefully acknowledged for the XPS measurement. The authors are very grateful to Leif Nyholm and Kristina Edström for their helpful discussion.

Appendix A. Supplementary data

Supplementary data related to this article can be found at http://dx.doi.org/10.1016/j.jpowsour.2015.12.074.

References

[1] H. Wang, Y. Yang, Y. Liang, G. Zheng, Y. Li, Y. Cui, H. Dai, Energy & Environ. Sci. 5 (2012) 7931–7935.

[2] J. Liu, M. Roberts, R. Younesi, M. Dahbi, K. Edström, T. Gustafsson, J. Zhu, J. Phys. Chem. Lett. 4 (2013) 4045–4050.
[4] D. Sun, Y. Shen, W. Zhang, L. Yu, Z. Yi, W. Yin, D. Wang, Y. Huang, J. Wang, D. Wang, J.B. Goodenough, 136 (2014) 8941–8946.
[5] Y. Shen, D. Sun, L. Yu, W. Zhang, Y. Shang, H. Tang, J. Wu, A. Cao, Y. Huang, Carbon 62 (2013) 288–295.
[6] Z. Jian, P. Liu, F. Li, P. He, X. Guo, M. Chen, H. Zhou, 53 (2014) 442–446.
[8] Y. Shao, F. Ding, J. Xiao, J. Zhang, W. Xu, S. Park, J.-G. Zhang, Y. Wang, J. Liu, 23 (2013) 987–1004.
[9] P. Trogadas, T.F. Fuller, P. Strasser, Carbon 75 (2014) 5–42.
[10] M.M. Ottakam Thotiyl, S.A. Freunberger, Z. Peng, P.G. Bruce, J. Am. Chem. Soc. 135 (2013) 494–500.
[11] R.E. Fuentes, H.R. Colón-Mercado, E.B. Fox, J. Power Sources 255 (2014) 219–222.
[12] S.Y. Kim, H.T. Lee, K.B. Kim, Phys. Chem. Chem. Phys. PCCP 15 (2013) 20262–20271.
[13] J. Kang, O.L. Li, N. Saito, 261 (2014) 156–161.
[14] S. Wang, X. Zhao, T. Cochell, A. Manthiram, J. Phys. Chem. Lett. 3 (2012) 2164–2167.
[15] Y. Lu, Z. Wen, J. Jin, Y. Cui, M. Wu, S. Sun, J. Solid State Electrochem. 16 (2012) 1863–1868.
[16] K. Zhang, L. Zhang, X. Chen, X. He, X. Wang, S. Dong, L. Gu, Z. Liu, C. Huang, G. Cui, ACS Appl. Mater. Interfaces 5 (2013) 3677–3682.
[17] L. Li, A. Manthiram, 4 (2014) 130175.
[18] X. Lin, X. Lu, T. Huang, Z. Liu, A. Yu, 242 (2013) 855–859.
[19] Z. Wang, X. Xiong, L. Qie, Y. Huang, Electrochimica Acta 106 (2013) 320–326.
[20] H. Li, W. Kang, L. Wang, Q. Yue, S. Xu, H. Wang, J. Liu, Carbon 54 (2013) 249–257.
[21] R. Mi, H. Liu, H. Wang, K.-W. Wong, J. Mei, Y. Chen, W.-M. Lau, H. Yan, Carbon 67 (2014) 744–752.
[22] W.H. Shin, H.M. Jeong, B.G. Kim, J.K. Kang, J.W. Choi, Nano Lett. 12 (2012) 2283–2288.
[23] Z. Wang, L. Qie, L. Yuan, W. Zhang, X. Hu, Y. Huang, Carbon 55 (2013) 328–334.
[24] Z. Chen, A. Yu, D. Higgins, H. Li, H. Wang, Z. Chen, Nano Lett. 12 (2012) 1946–1952.
[25] Z.-L. Wang, D. Xu, J.-J. Xu, L.-L. Zhang, X.-B. Zhang, 22 (2012) 3699–3705.
[27] W. Zhang, J. Zhu, H. Ang, Y. Zeng, N. Xiao, Y. Gao, W. Liu, H.H. Hng, Q. Yan, Nanoscale 5 (2013) 9651–9658.
[28] T. Cetinkaya, S. Ozcan, M. Uysal, M.O. Guler, H. Akbulut, J. Power Sources 267 (2014) 140–147.
[29] Z. Jian, Y. Chen, F. Li, T. Zhang, C. Liu, H. Zhou, J. Power Sources 251 (2014) 466–469.
[30] Z. Wang, P. Tammela, P. Zhang, M. Strømme, L. Nyholm, J. Mater. Chem. A 2 (2014) 16761–16769.
[31] Z. Wang, P. Tammela, P. Zhang, J. Huo, F. Ericson, M. Stromme, L. Nyholm, 6 (2014) 13068–13075.
[32] L. Nyholm, G. Nyström, A. Mihranyan, M. Strømme, 23 (2011) 3751–3769.
[33] P. Tammela, Z. Wang, S. Frykstrand, P. Zhang, I.-M. Sintorn, L. Nyholm, M. Stromme, RSC Adv. 5 (2015) 16405–16413.
[34] A. Naseem, C.J. Olliff, L.G. Martini, A.W. Lloyd, Int. J. Pharm. 269 (2004) 443–450.
[35] T. Fu, R. Liu, J. Lv, Z. Li, Fuel Process. Technol. 122 (2014) 49–57.
[36] P. Veselá, V. Slovák, J. Therm. Anal. Calorim. 113 (2013) 209–217.
[37] M. Reuß, L. Ratke, J. Sol-Gel Sci. Technol. 47 (2008) 74–80.
[38] C. Lin, J.A. Ritter, Carbon 35 (1997) 1271–1278.
[39] X. Yang, W. Zou, Y. Su, Y. Zhu, H. Jiang, J. Shen, C. Li, J. Power Sources 266 (2014) 36–42.
[40] F. Li, Y. Chen, D.-M. Tang, Z. Jian, C. Liu, D. Golberg, A. Yamada, H. Zhou, Energy Environ. Sci. 7 (2014) 1648.
[41] W. Luo, B. Wang, C.G. Heron, M.J. Allen, J. Morre, C.S. Maier, W.F. Stickle, X. Ji, Nano Lett. 14 (2014) 2225–2229.
[42] D. Yu, Q. Zhang, L. Dai, J. Am. Chem. Soc. 132 (2010) 15127–15129.
[43] H. Wang, T. Maiyalagan, X. Wang, ACS Catal. 2 (2012) 781–794.
[44] W. Liang, J. Chen, Y. Liu, S. Chen, ACS Catal. 4 (2014) 4170–4177.
[45] L. Zhang, J. Niu, L. Dai, Z. Xia, Langmuir 28 (2012) 7542–7550.
[46] F. Li, T. Zhang, H. Zhou, Energy Environ. Sci. 6 (2013) 1125–1141.
[47] M.M.O. Thotiyl, S.A. Freunberger, Z. Peng, Y. Chen, Zheng Liu, P.G. Bruce, Nat. Mater. 12 (2013) 1051–1056.
[48] D. Sharon, M. Afri, M. Noked, A. Garsuch, A.A. Frimer, D. Aurbach, J. Phys. Chem. Lett. 4 (2013) 3115–3119.
[49] A.C. Luntz, B.D. McCloskey, Chem. Rev. 114 (2014) 11721–11750.
[50] F. Li, T. Zhang, H. Zhou, Energy Environ. Sci. 6 (2013) 1125–1141.
[51] J. Liu, R. Younesi, T. Gustafsson, K. Edström, J. Zhu, Nano Energy 10 (2014) 19–27.
[52] Z. Peng, S.A. Freunberger, Y. Chen, P.G. Bruce, Science 337 (2012) 563–566.